Scientia Iranica A (2022) 29(6), 2825–2836

Sharif University of Technology
Scientia Iranica
Transactions A: Civil Engineering
http://scientiairanica.sharif.edu

Time harmonic analysis of concrete arch dam-reservoir systems utilizing GN high-order truncation condition

V. Lotfi[a,*] and A. Lotfi[b]

a. *Department of Civil and Environmental Engineering, Amirkabir University of Technology, Tehran, Iran.*
b. *Department of Mathematics, University of Colorado, Boulder, Colorado, USA.*

Received 16 November 2020; received in revised form 8 September 2021; accepted 7 March 2022

KEYWORDS
Concrete arch dams;
GN high-order condition;
Givoli-Neta condition;
Absorbing boundary conditions;
Truncation boundary.

Abstract. The present study formulates the dynamic analysis of concrete arch dam-reservoir systems using FE-(FE-TE) approach. In this technique, dam and reservoir are discretized by solid and fluid finite elements. Moreover, the GN high-order condition is imposed at the reservoir truncation boundary. This task is formulated by employing a truncation element at that boundary. It is emphasized that reservoir far-field is excluded from the discretized model. The formulation is initially explained in detail. Subsequently, the response of the idealized Morrow Point arch dam-reservoir system is obtained for two conditions of fully reflective and absorptive reservoir bottom/sidewalls for all three types of excitations. Different orders of GN condition are considered and convergence process is evaluated. Furthermore, the results are compared against exact solutions which are based on rigorous FE-(FE-HE) approach. It is shown that the technique reaches convergence prior to the beginning of instability problems known to exist for high orders in GN condition. It must be emphasized that although time harmonic analysis is considered in the present study, the main part of formulation is explained in the context of time domain. Therefore, the approach can easily be extended for transient type of analysis.

1. Introduction

It is a well-known fact for dam specialists that dynamic analysis of concrete arch dam-reservoir systems can be carried out rigorously by FE-(FE-HE) method in the frequency domain. This means that the dam is discretized by solid finite elements, while the reservoir is divided into two parts, a near-field region (usually an irregular shape) in the vicinity of the dam and a far-field part (assuming uniform channel) which extends to infinity in the upstream direction. The former region is discretized by fluid finite elements, while the latter is modeled by a three-dimensional fluid hyper element [1–5]. It is also understood that employing fluid hyper-elements would lead to the exact solution (in numerical sense) of the problem. However, it is formulated in the frequency domain and its application in this field has led to many special-purpose programs that were demanding from programming point of view.

Furthermore, engineers have often tried to solve this problem in the context of pure finite element programming (FE-FE method of analysis). In this approach, an often-simplified condition is imposed on the truncation boundary or the upstream face of the near-field water domain. Thus, the fluid hyper-element is actually excluded from the model. Two of these widely used methods are based on Sommerfeld and Sharan (more accurately, modified-Sharan condition adjusted for three-dimensional cases) truncation boundary conditions [6,7]. The main advantage of

*. *Corresponding author.*
E-mail addresses: vahlotfi@aut.ac.ir (V. Lotfi); Ali.Lotfi@colorado.edu (A. Lotfi)

doi: 10.24200/sci.2022.57180.5102

these conditions is that it can be readily used for time domain analysis. Thus, they are also vastly employed in nonlinear seismic analysis of concrete dams. However, their major shortcoming is that the results have significant errors when low normalized reservoir lengths (in the order of $L/H = 1$) are utilized.

Of course, there have also been many researches in the last three decades to develop more accurate absorbing boundary conditions to be applied for similar fluid-structure or soil-structure interaction problems. It should be emphasized that many of these studies have actually limited their works to two-dimensional cases. Perfectly matched layer [8-15] and high-order non-reflecting boundary condition [16-22] are among the two main popular groups of methods that researchers have applied in their attempts. It is emphasized that these techniques have become very popular in recent years given that they could be applied in time domain as well as the frequency domain.

The present study proposed formulation based on FE-(FE-TE) procedure for dynamic analysis of concrete arch dam-reservoir systems. The technique is described in great detail. The core of the method is based on utilizing a truncation element at the U/S truncation boundary of the reservoir near-field domain and excluding the far-field region of the reservoir. This truncation element is formulated based on the GN-type high-order condition applied at that boundary. Moreover, a special-purpose finite element program is enhanced for this investigation based on the explained formulation. Thereafter, the response of idealized Morrow Point arch dam is studied due to stream, vertical, and cross-stream ground motions. Several cases are defined by changing the GN condition order and the convergence process is studied. Moreover, two conditions of fully reflective and absorptive reservoir bottom/sidewalls are considered.

The results are also compared for different cases against the corresponding exact responses that are obtained by the rigorous FE-(FE-HE) type of analysis.

It should be also emphasized that the present formulation allows one to readily apply it for transient type of analysis. However, it was decided that the formulation would be applied presently for time harmonic excitation to ensure a better evaluation of convergence process and proof of its effectiveness independent of any specified earthquake excitation.

It is also worthwhile to mention that the Morrow Point arch dam considered herein has been investigated thoroughly in many recent studies. Some of these works relate to linear analysis by Wavenumber approach [23], direct finite element method [24,25], or HW high-order boundary condition [26]. There are others related to nonlinear response [27], modal identification [28], or even mode shapes of this particular dam [29].

2. Method of analysis

As mentioned, the analysis technique utilized in this study is based on the FE-(FE-TE) method, which is applicable to a general concrete arch dam-reservoir system. The coupled equations can be obtained by considering each region separately and then, the resulting equations are combined.

2.1. Dam body

Upon concentrating on the structural part, the dynamic behavior of the dam is described by the well-known equation of structural dynamics [30]:

$$\mathbf{M}\ddot{\mathbf{r}} + \mathbf{C}\dot{\mathbf{r}} + \mathbf{K}\mathbf{r} = -\tilde{\mathbf{M}}\mathbf{J}\mathbf{a}_g + \mathbf{B}^T\mathbf{P}, \tag{1}$$

where $\mathbf{M}$, $\mathbf{C}$, and $\mathbf{K}$ in this relation represent the mass, damping, and stiffness matrices of the dam body. Moreover, $\mathbf{r}$ is the vector of nodal relative displacements, $\tilde{\mathbf{M}}$ is the same as $\mathbf{M}$ matrix except that no columns are excluded due to restraints, $\mathbf{J}$ is a matrix with each of three rows equal to a 3×3 identity matrix (its columns correspond to unit cross-stream, stream, and vertical rigid body motion), and $\mathbf{a}_g$ denotes the vector of ground accelerations. Furthermore, $\mathbf{B}$ is a matrix that relates vectors of hydrodynamic pressures (i.e., $\mathbf{P}$) and its equivalent nodal forces. It should be also emphasized that $\mathbf{a}_g$ denotes the vector of ground accelerations in three directions.

2.2. Water domain

Upon applying the weighted residual approach to the governing equation of water region (i.e., wave equation [31,32]), the finite element equation of the reservoir is obtained, which may be written as:

$$\mathbf{G}\ddot{\mathbf{P}} + q\mathbf{L}_{II}\dot{\mathbf{P}} + \mathbf{H}\mathbf{P} = \mathbf{R}_I - \mathbf{B}\ddot{\mathbf{r}} - \tilde{\mathbf{B}}\mathbf{J}\mathbf{a}_g. \tag{2}$$

In this relation, $\mathbf{G}$ $\mathbf{H}$ are the generalized mass and stiffness matrices of the fluid domain and $\mathbf{P}$ is the vector of nodal pressures. Of note, all boundary conditions are already considered in Eq. (2). In particular, the one related to the reservoir's bottom/sidewalls surface (i.e., Γ_{II}; Figure 1), dam-reservoir's interface (i.e., Γ_{III}), water surface, and the contribution related to the truncation boundary condition is symbolically denoted by the vector $\mathbf{R}_I$. It should be mentioned that admittance or damping coefficient q utilized in the above equation may be related to a more meaningful wave reflection coefficient α [33]:

$$\alpha = \frac{1 - q\,c}{1 + q\,c}, \tag{3}$$

which is defined as the ratio of the amplitude of reflected hydrodynamic pressure wave to the amplitude of incident pressure wave normal to the reservoir's bottom/sidewalls. For a fully reflective reservoir's bottom/sidewalls condition, α is equal to 1 which leads

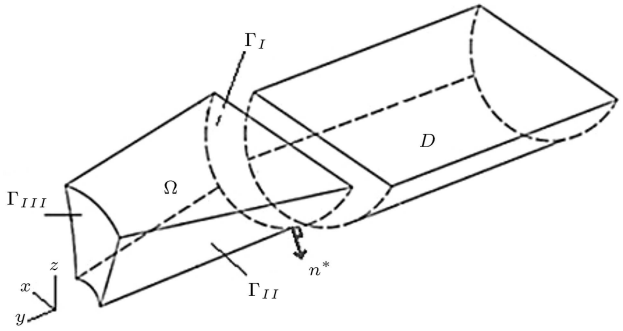

Figure 1. Schematic view of a typical reservoir (i.e., water domain). The near-field reservoir domain Ω, the truncation boundary Γ_I, and the far-field region D (excluded in the FE-(FE-TE) type of analysis).

to $q = 0$. It is also noted that parameter c corresponds to water pressure wave velocity.

Furthermore, matrix $\mathbf{B}$ in Eq. (2) results from the dam-reservoir boundary condition that also appears in Eq. (1). Matrix $\tilde{\mathbf{B}}$ is the same as matrix $\mathbf{B}$, except that no columns are excluded due to restraints, and it has contributions due to reservoir bottom/sidewalls as well as the dam-reservoir interface. Moreover, the vector $\mathbf{R}_I$ of the truncation boundary is obtained by assembling the following boundary integrals of the fluid elements adjacent to that surface (i.e., Γ_I):

$$\mathbf{R}^e = \frac{1}{\rho}\int_{\Gamma^e} \mathbf{N}\,(\partial_n P)\,d\Gamma^e. \tag{4}$$

With $\mathbf{N}$ being the vector of element's shape functions, ρ is the water density, and n denotes the fluid element's outward normal direction.

2.3. Dam-reservoir system

The necessary equations for both dam and reservoir domains were explained in previous sections. Thus, combination of the main relations (1) and (2) would result in the FE equations of the coupled dam-reservoir system in its initial form for the time domain:

$$\begin{pmatrix} \mathbf{M} & \mathbf{0} \\ \mathbf{B} & \mathbf{G} \end{pmatrix}\begin{pmatrix} \ddot{\mathbf{r}} \\ \ddot{\mathbf{P}} \end{pmatrix} + \begin{pmatrix} \mathbf{C} & \mathbf{0} \\ \mathbf{0} & q\mathbf{L}_{II} \end{pmatrix}\begin{pmatrix} \dot{\mathbf{r}} \\ \dot{\mathbf{P}} \end{pmatrix} + \begin{pmatrix} \mathbf{K} & -\mathbf{B}^T \\ \mathbf{0} & \mathbf{H} \end{pmatrix}\begin{pmatrix} \mathbf{r} \\ \mathbf{P} \end{pmatrix} + \begin{pmatrix} \mathbf{0} \\ -\mathbf{R}_I \end{pmatrix} = \begin{pmatrix} -\tilde{\mathbf{M}}\mathbf{J}\mathbf{a}_g \\ -\tilde{\mathbf{B}}\mathbf{J}\mathbf{a}_g \end{pmatrix}. \tag{5}$$

It is noted from the above equation that vector $\mathbf{R}_I$ still needs to be defined by some appropriate condition. This is related to the truncated boundary Γ_I. It is interesting to note that one may presume that there exists a truncation-element attached at this boundary similar to hyper-element. The purpose of this element is to produce the vector $\mathbf{R}_I$ based on the GN high-order boundary condition. The element will have generalized mass, damping, and stiffness matrices similar to usual solid or fluid finite elements. The details are discussed below.

2.4. Definition of $\mathbf{R}_I$ vector for general excitations

The effect of truncation boundary condition will be treated in this section. For this purpose, let us now assume that this boundary (i.e., Γ_I) is parallel to $x-z$ plane (Figure 1). It is apparent that $\mathbf{R}_I$ vector is obtained by assemblage of contributions from different fluid finite elements (i.e., $\mathbf{R}_I^e$). To this end, one may utilize Eq. (4) to obtain $\mathbf{R}_I^e$, if there is merely stream excitation (i.e., y-direction in Figure 2(b)). However, the following equation must be employed in general conditions where vertical (i.e., z-direction) or cross-

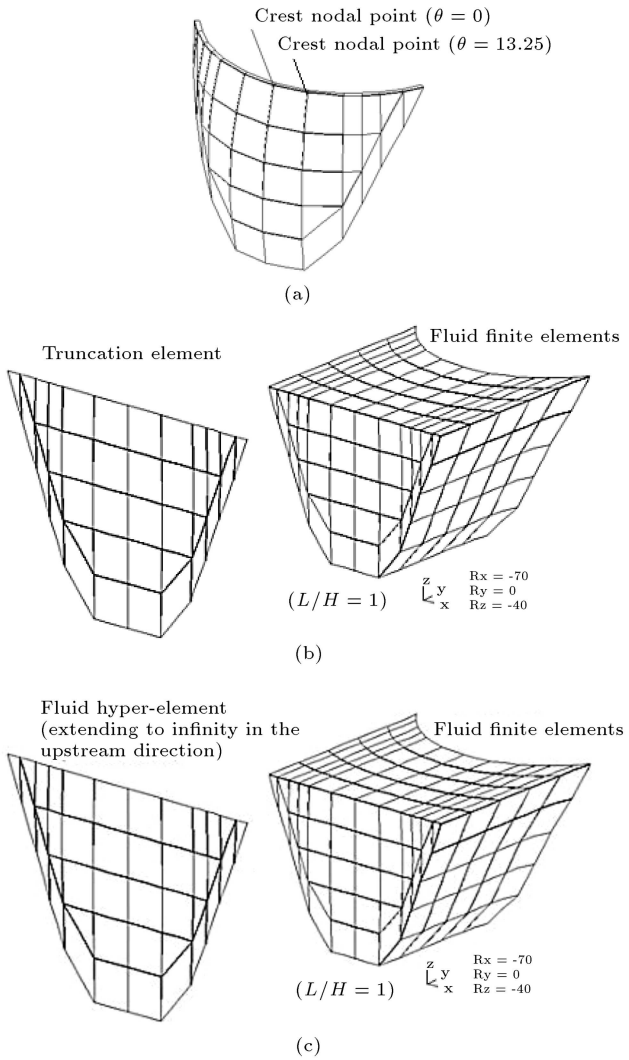

Figure 2. Discretization of dam-reservoir system: (a) Dam body, (b) water domain for FE-(FE-TE) model (fluid finite elements ($L/H = 1$), and the truncation element), and (c) water domain for FE-(FE-HE) model (fluid finite elements ($L/H = 1$), and the fluid hyper-element).

stream excitations (i.e., x-direction) may also exist:

$$\mathbf{R}_I^e = \frac{1}{\rho}\int_{\Gamma_I^e} \mathbf{N}\left(\partial_n P^s\right) d\Gamma^e. \tag{6}$$

It is noted that P^s (scattered pressure) term is substituted for P (total pressure) and they are related as follows:

$$P^s = P - P^i. \tag{7}$$

P^i is the incidence pressure contribution that is due to ground acceleration imposed at bottom/side-walls of uniform channel extending to infinity in the upstream direction (Figure 1). It is noted that this portion is actually eliminated in our current discretization since it is beyond the truncation boundary. However, the impact of incidence pressure is included in the present FE-FE approach through Eqs. (6) and (7).

Now, P^s is substituted by another function ϕ_0 which is utilized in writing the GN high-order boundary condition later on:

$$\phi_0 = P^s. \tag{8}$$

Employing this function, Eq. (6) may be rewritten as follows:

$$\mathbf{R}_I^e = \frac{1}{\rho}\int_{\Gamma_I^e} \mathbf{N}\left(-\partial_y \phi_0\right) d\Gamma^e. \tag{9}$$

It is noted that the negative sign in this relation is due to the fact that the outward normal is opposite to the y-direction for fluid finite elements adjacent to the truncation boundary (Figure 1). It is obvious that simplified relations (e.g., Sommerfeld condition) may be utilized in Eq. (9) to explicitly define that vector. However, that would not produce accurate results for low values of normalized reservoir length as previously mentioned. Therefore, one would prefer to resort to high-order conditions as presented in the next section.

3. GN type truncation-element

3.1. Extraction of basic relations

As mentioned, high-order conditions are adopted herein for the truncation boundary. In particular, GN condition is employed in the present study [17]. This condition was initially written to absorb propagating waves at the applied boundary. However, that can be generalized to include also evanescent waves. Accordingly, one can write the GN condition of Order N, M (i.e., ON-M) in the following for the truncation boundary:

$$\left[\prod_{j=1}^{M}\left(c\,\partial_y - b_j\right)\right]\left[\prod_{j=1}^{N}\left(c\,\partial_y - a_j\partial_t\right)\right]\phi_0 = 0. \tag{10}$$

Alternatively, it may be written in a more simplified form:

$$\left[\prod_{j=1}^{M}\left(\partial_y - \bar{b}_j\right)\right]\left[\prod_{j=1}^{N}\left(\partial_y - \bar{a}_j\partial_t\right)\right]\phi_0 = 0, \tag{11}$$

with the following definitions for normalized coefficients $\bar{a}_j$ and $\bar{b}_j$:

$$\bar{a}_j = \frac{a_j}{c}; \qquad j = 1,\ldots,N, \tag{12a}$$

$$\bar{b}_j = \frac{b_j}{c}; \qquad j = 1,\ldots,M, \tag{12b}$$

where c is the pressure wave velocity of fluid. Obviously, Eq. (11) may also be written similar to its initial form [17]:

$$\left[\prod_{j=1}^{M+N}\left(\partial_y - \bar{a}_j\partial_t\right)\right]\phi_0 = 0. \tag{13}$$

However, one should employ the following relation in that transformation:

$$\bar{b}_j = \bar{a}_{N+j}\partial_t; \qquad j = 1,\ldots,M. \tag{14}$$

Of course, Eq. (13) may also be written as follows by defining auxiliary functions $\phi_j\left(x,y,z\right)$:

$$\phi_j = \left(\partial_y - \bar{a}_j\partial_t\right)\phi_{j-1}; \quad j = 1,\ldots,M+N, \tag{15}$$

$$\phi_{M+N} = 0. \tag{16}$$

It is recalled that ϕ_0 is the same as function P^s (scattered pressure wave) which itself should satisfy the governing wave equation in the fluid domain. Therefore, all auxiliary functions ϕ_j would also satisfy a similar equation, since they are related through an operator as easily verified in Eq. (15):

$$\nabla^2\phi_j = \bar{c}^2\,\ddot{\phi}_j; \quad \bar{c} = \frac{1}{c}. \tag{17}$$

Moreover, these auxiliary functions should satisfy boundary conditions at intersection between truncation surface and reservoir bottom/side-walls of the canyon similar to ϕ_0:

$$\partial_{n^*}\phi_j = -q\partial_t\phi_j. \tag{18}$$

It is worthwhile to emphasize that n^* is normal to that intersection boundary in $x-z$ plane (curved line, Figure 1) and admittance coefficient q is related to reflection coefficient α through Eq. (3).

According to Eq. (15), one can also define the first partial derivative of function ϕ_{j-1} as:

$$\partial_y\phi_{j-1} = \phi_j + \bar{a}_j\partial_t\phi_{j-1}; \quad j = 1,\ldots,M+N. \tag{19}$$

Now, the operator ∂_y should be applied to Eq. (15) which yields:

$$\partial_y\phi_j = \left(\partial_y^2 - \bar{a}_j\,\partial_{yt}\right)\phi_{j-1}. \tag{20}$$

Utilizing Eq. (19) for j and $j-1$ in Eq. (20) results in:

$$\phi_{j+1} + \bar{a}_{j+1}\partial_t\phi_j = \partial_y^2\phi_{j-1} - \bar{a}_j\partial_t\left(\phi_j + \bar{a}_j\partial_t\phi_{j-1}\right), \tag{21}$$

which may be rewritten as follows:

$$\bar{a}_j^2\partial_t^2\phi_{j-1} - \partial_y^2\phi_{j-1} + (\bar{a}_j + \bar{a}_{j+1})\partial_t\phi_j + \phi_{j+1} = 0. \tag{22}$$

By employing Eq. (17) for $j-1$, Eq. (22) is transformed as:

$$(\bar{a}_j^2 - \bar{c}^2)\,\ddot{\phi}_{j-1} + \left(\partial_x^2 + \partial_z^2\right)\phi_{j-1} + (\bar{a}_j + \bar{a}_{j+1})\,\partial_t\phi_j + \phi_{j+1} = 0. \tag{23}$$

At this point, the weighted residual approach is applied to Eq. (23) by multiplying it by a weighting function w and integrating it with the truncation boundary for each fluid finite element.

$$\frac{1}{\rho}\int_A w[(\bar{a}_j^2 - \bar{c}^2)\,\ddot{\phi}_{j-1} + \left(\partial_x^2 + \partial_z^2\right)\phi_{j-1} + (\bar{a}_j + \bar{a}_{j+1})\,\partial_t\phi_j + \phi_{j+1}]\,dxdz = 0. \tag{24}$$

This may also be visualized as integration on the surface of each sub-element of the truncation-element that is going to augment our model at the truncation boundary. Interpolation of functions in Eq. (24) leads to the following matrix equation for each sub-element:

$$\begin{aligned}(\bar{a}_j^2 - \bar{c}^2)&\left(\frac{1}{\rho}\int_A \mathbf{N}\mathbf{N}^{\mathrm{T}}dA\ddot{\mathbf{\Phi}}_{j-1}^e\right) + \left(\frac{1}{\rho}\int_s \mathbf{N}\partial_{n^*}\phi_{j-1}ds\right)\\ &- \left(\frac{1}{\rho}\int_A \left(\mathbf{N}_x\mathbf{N}_x^T + \mathbf{N}_z\mathbf{N}_z^T\right)dA\dot{\mathbf{\Phi}}_{j-1}^e\right)\\ &+ (\bar{a}_j + \bar{a}_{j+1})\left(\frac{1}{\rho}\int_A \mathbf{N}\mathbf{N}^T dA\dot{\mathbf{\Phi}}_j^e\right)\\ &+ \left(\frac{1}{\rho}\int_A \mathbf{N}\mathbf{N}^T dA\mathbf{\Phi}_{j+1}^e\right) = 0.\end{aligned} \tag{25}$$

This relation can be written in a more simplified form as follows:

$$(\bar{a}_j^2 - \bar{c}^2)\mathbf{L}_I^e\ddot{\mathbf{\Phi}}_{j-1}^e - \mathbf{Q}_I^e\dot{\mathbf{\Phi}}_{j-1}^e - \mathbf{D}_I^e\mathbf{\Phi}_{j-1}^e + (\bar{a}_j + \bar{a}_{j+1})\mathbf{L}_I^e\dot{\mathbf{\Phi}}_j^e + \mathbf{L}_I^e\mathbf{\Phi}_{j+1}^e = 0. \tag{26}$$

By utilizing the following matrix definitions, we have:

$$\mathbf{L}_I^e = \frac{1}{\rho}\int_A \mathbf{N}\mathbf{N}^T dA, \tag{27a}$$

$$\mathbf{Q}_I^e = \frac{q}{\rho}\int_s \mathbf{N}\mathbf{N}^T ds, \tag{27b}$$

$$\mathbf{D}_I^e = \frac{1}{\rho}\int_A \left(\mathbf{N}_x\mathbf{N}_x^T + \mathbf{N}_z\mathbf{N}_z^T\right)dA. \tag{27c}$$

Assembling Eq. (26) for different sub-elements would lead to the following relation, which is valid for the truncation element.

$$(\bar{a}_j^2 - \bar{c}^2)\mathbf{L}_I\ddot{\mathbf{\Phi}}_{j-1} - \mathbf{Q}_I\dot{\mathbf{\Phi}}_{j-1} - \mathbf{D}_I\mathbf{\Phi}_{j-1} + (\bar{a}_j + \bar{a}_{j+1})\mathbf{L}_I\dot{\mathbf{\Phi}}_j + \mathbf{L}_I\mathbf{\Phi}_{j+1} = 0, \quad j = 1, ..., M+N-1. \tag{28}$$

These relations hold at different j values and the last auxiliary vector must be a null vector:

$$\mathbf{\Phi}_{N+M} = 0. \tag{29}$$

Eq. (28) are valid when all terms would be devised for propagating waves in GN condition as in Eq. (13). However, these relations are changed for certain j values when there are N and M propagating and evanescent terms, respectively, as in Eq. (11). Under these circumstances, Eq. (28) may be written at different j values as follows:

$$(\bar{a}_j^2 - \bar{c}^2)\mathbf{L}_I\ddot{\mathbf{\Phi}}_{j-1} - \mathbf{Q}_I\dot{\mathbf{\Phi}}_{j-1} - \mathbf{D}_I\mathbf{\Phi}_{j-1} + (\bar{a}_j + \bar{a}_{j+1})\mathbf{L}_I\dot{\mathbf{\Phi}}_j + \mathbf{L}_I\mathbf{\Phi}_{j+1} = 0, \quad j = 1, .., N-1, \tag{30}$$

$$(\bar{a}_N^2 - \bar{c}^2)\mathbf{L}_I\ddot{\mathbf{\Phi}}_{N-1} - \mathbf{Q}_I\dot{\mathbf{\Phi}}_{N-1} - \mathbf{D}_I\mathbf{\Phi}_{N-1} + \bar{a}_N\mathbf{L}_I\dot{\mathbf{\Phi}}_N + \bar{b}_1\mathbf{L}_I\mathbf{\Phi}_N + \mathbf{L}_I\mathbf{\Phi}_{N+1} = 0, \tag{31}$$

$$-\bar{c}^2\mathbf{L}_I\ddot{\mathbf{\Phi}}_{N+k-1} + \bar{b}_k^2\mathbf{L}_I\mathbf{\Phi}_{N+k-1} - \mathbf{Q}_I\dot{\mathbf{\Phi}}_{N+k-1} - \mathbf{D}_I\mathbf{\Phi}_{N+k-1} + (\bar{b}_k + \bar{b}_{k+1})\mathbf{L}_I\mathbf{\Phi}_{N+k} + \mathbf{L}_I\mathbf{\Phi}_{N+k+1} = 0; \quad k = 1, .., M-1 \text{ or } j = N+1, .., N+M-1. \tag{32}$$

It is worthwhile to mention that Eqs. (31) and (32) are transformed from Eq. (28) by employing Relation (14). Moreover, the last auxiliary vector should also satisfy Eq. (29), as mentioned previously.

Apart from the above basic equations, certain other relations are required, which are discussed in the next sub-sections.

3.2. Explicit form of $\mathbf{R}_I$ *vector*

The original objective of introducing truncation-element is to calculate $\mathbf{R}_I$ term in Eq. (5). Subsection 2.4 made a reference to the procedure to calculate $\mathbf{R}_I$ vector under general conditions. This task will be completed in the present subsection. For this purpose,

one may substitute $\partial_y\phi_0$ in Eq. (9) by employing Eq. (19) for $j=1$ which yields:

$$\mathbf{R}_I^e = \frac{1}{\rho}\int_{\Gamma_I^e} \mathbf{N}\left(-\bar{a}_1\,\dot{\phi}_0 - \phi_1\right) d\Gamma^e. \tag{33}$$

This relation may also be visualized as being pertinent to each sub-element of the truncation-element. By interpolating functions $\dot{\phi}_0$ and ϕ_1 using shape functions, the above relation can be written into the following relation:

$$\mathbf{R}_I^e = -\bar{a}_1\mathbf{L}_I^e\dot{\mathbf{\Phi}}_0^e - \mathbf{L}_I^e\mathbf{\Phi}_1^e. \tag{34}$$

Assembling these vectors results in:

$$\mathbf{R}_I = -\bar{a}_1\mathbf{L}_I\dot{\mathbf{\Phi}}_0 - \mathbf{L}_I\mathbf{\Phi}_1. \tag{35}$$

Of note, ϕ_0 (equivalent to P^s) may be replaced through Eq. (7). Therefore, one would obtain:

$$\mathbf{R}_I + \bar{a}_1\mathbf{L}_I\left(\dot{\mathbf{P}} - \dot{\mathbf{P}}^i\right) + \mathbf{L}_I\mathbf{\Phi}_1 = 0. \tag{36}$$

3.3. Complementary relation to define incidence pressure wave vector

It was noticed that the incidence pressure wave vector ($\mathbf{P}^i$) was introduced to Eq. (36). Therefore, this vector is also required to be defined through another complementary relation, which is discussed in this subsection.

The incidence pressure wave function obeys the following governing equation:

$$+\bar{c}^2\ddot{P}^i - \left(\partial_x^2 + \partial_z^2\right)P^i = 0. \tag{37}$$

This is apparent since it is a function independent of y direction. Moreover, apart from the top surface condition ($P^i = 0$), it should satisfy the following boundary condition:

$$\partial_{n^*}P^i = -q\,P^i - \rho\,a_g^{n^*}. \tag{38}$$

Now, we apply the weighted residual approach to Eq. (37) by multiplying this relation by weighting function w and integrating it for each sub-element of truncation-element. This is written as:

$$\frac{1}{\rho}\int_A w\left(+\bar{c}^2\ddot{P}^i - \left(\partial_x^2 + \partial_z^2\right)P^i\right) = 0. \tag{39}$$

Interpolating w, P^i, and $\ddot{P}^i$ in Eq. (39) by employing shape functions will lead to the following relation, which is true for each sub-element:

$$\bar{c}^2\left(\frac{1}{\rho}\int_A \mathbf{N}\mathbf{N}^T dA\right)\ddot{\mathbf{P}}^{ie} + \left(\frac{1}{\rho}\int_A\left(\mathbf{N}_x\mathbf{N}_x^T + \mathbf{N}_z\mathbf{N}_z^T\right)dA\right)\mathbf{P}^{ie} - \frac{1}{\rho}\int_s \mathbf{N}\left(\partial_{n^*}P^i\right)ds = \mathbf{0}. \tag{40}$$

This relation may be rewritten by employing Eqs. (27) and (38):

$$\bar{c}^2\mathbf{L}_I^e\ddot{\mathbf{P}}^{ie} + \mathbf{D}_I^e\mathbf{P}^{ie} - \frac{1}{\rho}\int_s \mathbf{N}\left(-qP^i - \rho\,a_g^{n^*}\right)ds = \mathbf{0}. \tag{41}$$

Furthermore, P^i may be interpolated by the help of shape functions and $a_g^{n^*}$ is written in terms of ground acceleration vector. Thus, one obtains:

$$\bar{c}^2\mathbf{L}_I^e\ddot{\mathbf{P}}^{ie} + \mathbf{D}_I^e\mathbf{P}^{ie} + \mathbf{Q}_I^e\dot{\mathbf{P}}^{ie} = -\left(\int_s \mathbf{N}\begin{pmatrix} n_x^* & 0 & n_z^*\end{pmatrix}ds\right)\mathbf{a}_g. \tag{42}$$

It is further simplified as:

$$\bar{c}^2\mathbf{L}_I^e\ddot{\mathbf{P}}^{ie} + \mathbf{D}_I^e\mathbf{P}^{ie} + \mathbf{Q}_I^e\dot{\mathbf{P}}^{ie} = -\mathbf{E}_I^{ie}\mathbf{a}_g, \tag{43}$$

by utilizing following matrix definition:

$$\mathbf{E}_I^{ie} = \int_s \mathbf{N}\begin{pmatrix} n_x^* & 0 & n_z^*\end{pmatrix}ds. \tag{44}$$

It should be noted that Eq. (43) is true for each sub-element and the right-hand side exists only for sub-elements adjacent to canyon boundary. Assembling it would lead to:

$$\bar{c}^2\mathbf{L}_I\ddot{\mathbf{P}}^i + \mathbf{Q}_I\dot{\mathbf{P}}^i + \mathbf{D}_I\mathbf{P}^i = -\mathbf{E}_I^i\mathbf{a}_g. \tag{45}$$

3.4. Generalized matrices of GN type truncation-element

Eq. (45) is the last required matrix relation for GN-type truncation-element. Therefore, a complete equation set is obtained that comprises Eqs. (30), (31), (32), (36) and (45). It is again emphasized that the last auxiliary vector in Eq. (32) should satisfy Eq. (29), which can be easily implemented in that equation. These relations are now written in the following compacted form:

$$\mathbf{M}_I\ddot{\mathbf{P}}_I + \mathbf{C}_I\dot{\mathbf{P}}_I + \mathbf{K}_I\mathbf{P}_I + \tilde{\mathbf{R}}_I = \mathbf{F}_I. \tag{46}$$

It is worthwhile to define the following vectors employed in Eq. (46):

$$\mathbf{P}_I = \begin{pmatrix}\mathbf{P}^T & \mathbf{\Phi}_1^T & \dots & \mathbf{\Phi}_N^T & \mathbf{\Phi}_{N+1}^T & \dots & \mathbf{\Phi}_{N+M-1}^T & \mathbf{P}^{iT}\end{pmatrix}^{\mathrm{T}}, \tag{47}$$

$$\tilde{\mathbf{R}}_I = \begin{pmatrix}\mathbf{R}_I^T & 0 & \dots & 0 & 0 & \dots & 0 & 0\end{pmatrix}^T, \tag{48}$$

$$\mathbf{F}_I = \begin{pmatrix}0 & 0 & \dots & 0 & 0 & \dots & 0 & \left(-\mathbf{E}_I^i\mathbf{a}_g\right)^T\end{pmatrix}^T. \tag{49}$$

Moreover, details of generalized matrices (i.e., $\mathbf{M}_I, \mathbf{C}_I, \mathbf{K}_I$) are provided in Tables 1-3.

Table 1. Explicit form of generalized matrix M_I.

	$\boldsymbol{P^T}$	$\boldsymbol{\phi_1^T}$	$\boldsymbol{\phi_2^T}$	$\boldsymbol{\phi_N^T}$	$\boldsymbol{\phi_{N-1}^T}$	$\boldsymbol{\phi_{N+M-2}^T}$	$\boldsymbol{\phi_{N+M-1}^T}$	$\boldsymbol{P^{iT}}$
$\boldsymbol{P}$	0	0	0	0	0	0	0	0
$\boldsymbol{\phi_1}$	$(\bar{a}_1^2-\bar{c}^2)\mathbf{L}_I$	0	0	0	0	0	0	$-(\bar{a}_1^2-\bar{c}^2)\mathbf{L}_I$
$\boldsymbol{\phi_2}$	0	$(\bar{a}_2^2-\bar{c}^2)\mathbf{L}_I$	0	0	0	0	0	0
$\boldsymbol{\phi_N}$	0	0	$(\bar{a}_N^2-\bar{c}^2)\mathbf{L}_I$	0	0	0	0	0
$\boldsymbol{\phi_{N+1}}$	0	0	0	$-\bar{c}^2\mathbf{L}_I$	0	0	0	0
$\boldsymbol{\phi_{N+M-2}^T}$	0	0	0	0	$-\bar{c}^2\mathbf{L}_I$	0	0	0
$\boldsymbol{\phi_{N+M-1}^T}$	0	0	0	0	0	$-\bar{c}^2\mathbf{L}_I$	0	0
$\boldsymbol{P^i}$	0	0	0	0	0	0	0	$\bar{c}^2\mathbf{L}_I$

Table 2. Explicit form of generalized matrix C_I.

	$\boldsymbol{P^T}$	$\boldsymbol{\phi_1^T}$	$\boldsymbol{\phi_2^T}$	$\boldsymbol{\phi_N^T}$	$\boldsymbol{\phi_{N-1}^T}$	$\boldsymbol{\phi_{N+M-2}^T}$	$\boldsymbol{\phi_{N+M-1}^T}$	$\boldsymbol{P^{iT}}$
$\boldsymbol{P}$	$\bar{a}_1\mathbf{L}_I$	0	0	0	0	0	0	$-\bar{a}_1\mathbf{L}_I$
$\boldsymbol{\phi_1}$	$-\mathbf{Q}_I$	$(\bar{a}_1+\bar{a}_2)\mathbf{L}_I$	0	0	0	0	0	$\mathbf{Q}_I$
$\boldsymbol{\phi_2}$	0	$-\mathbf{Q}_I$	$(\bar{a}_2+\bar{a}_3)\mathbf{L}_I$	0	0	0	0	0
$\boldsymbol{\phi_N}$	0	0	$-\mathbf{Q}_I$	$\bar{a}_N\mathbf{L}_I$	0	0	0	0
$\boldsymbol{\phi_{N+1}}$	0	0	0	$-\mathbf{Q}_I$	0	0	0	0
$\boldsymbol{\phi_{N+M-2}^T}$	0	0	0	0	$-\mathbf{Q}_I$	0	0	0
$\boldsymbol{\phi_{N+M-1}^T}$	0	0	0	0	0	$-\mathbf{Q}_I$	0	0
$\boldsymbol{P^i}$	0	0	0	0	0	0	0	$\mathbf{Q}_I$

Table 3. Explicit form of generalized matrix K_I.

	$\boldsymbol{P^T}$	$\boldsymbol{\phi_1^T}$	$\boldsymbol{\phi_2^T}$	$\boldsymbol{\phi_N^T}$	$\boldsymbol{\phi_{N-1}^T}$	$\boldsymbol{\phi_{N+M-2}^T}$	$\boldsymbol{\phi_{N+M-1}^T}$	$\boldsymbol{P^{iT}}$
$\boldsymbol{P}$	0	$\mathbf{L}_I$	0	0	0	0	0	0
$\boldsymbol{\phi_1}$	$-\mathbf{D}_I$	0	$\mathbf{L}_I$	0	0	0	0	$\mathbf{D}_I$
$\boldsymbol{\phi_2}$	0	$-\mathbf{D}_I$	0	$\mathbf{L}_I$	0	0	0	0
$\boldsymbol{\phi_N}$	0	0	$-\mathbf{D}_I$	$\bar{b}_1\mathbf{L}_I$	$\mathbf{L}_I$	0	0	0
$\boldsymbol{\phi_{N+1}}$	0	0	0	$\bar{b}_1^2\mathbf{L}_I-\mathbf{D}_I$	$\left(\bar{b}_1+\bar{b}_2\right)\mathbf{L}_I$	$\mathbf{L}_I$	0	0
$\boldsymbol{\phi_{N+M-2}^T}$	0	0	0	0	$\bar{b}_{M-2}^2\mathbf{L}_I-\mathbf{D}_I$	$\left(\bar{b}_{M-2}+\bar{b}_{M-1}\right)\mathbf{L}_I$	$\mathbf{L}_I$	0
$\boldsymbol{\phi_{N+M-1}^T}$	0	0	0	0	0	$\bar{b}_{M-1}^2\mathbf{L}_I-\mathbf{D}_I$	$\left(\bar{b}_{M-1}+\bar{b}_M\right)\mathbf{L}_I$	0
$\boldsymbol{P^i}$	0	0	0	0	0	0	0	$\mathbf{D}_I$

4. Coupled equations of dam-reservoir system

The matrix equation of the dam-reservoir system was already presented in Subsection 2.3 (i.e., Eq. (5)). Combining that equation with Eq. (46) would result in the coupled equation of dam-reservoir system in its final form:

$$\begin{pmatrix} \mathbf{M} & \mathbf{0} \\ \bar{\mathbf{B}} & \bar{\mathbf{G}}+\bar{\mathbf{M}}_I \end{pmatrix}\begin{pmatrix} \ddot{\mathbf{r}} \\ \ddot{\bar{\mathbf{P}}} \end{pmatrix}+\begin{pmatrix} \mathbf{C} & \mathbf{0} \\ \mathbf{0} & q\bar{\mathbf{L}}_{II}+\bar{\mathbf{C}}_I \end{pmatrix}\begin{pmatrix} \dot{\mathbf{r}} \\ \dot{\bar{\mathbf{P}}} \end{pmatrix}+\begin{pmatrix} \mathbf{K} & -\bar{\mathbf{B}}^T \\ \mathbf{0} & \bar{\mathbf{H}}+\bar{\mathbf{K}}_I \end{pmatrix}\begin{pmatrix} \mathbf{r} \\ \bar{\mathbf{P}} \end{pmatrix} = \begin{pmatrix} -\tilde{\mathbf{M}}\mathbf{J}\mathbf{a}_g \\ -\bar{\tilde{\mathbf{B}}}\,\mathbf{J}\mathbf{a}_g+\bar{\mathbf{F}}_I \end{pmatrix}. \tag{50}$$

It is noted that vectors $\tilde{\mathbf{R}}_I$ and $-\mathbf{R}_I$ cancel each other during this process. Furthermore, the bar sign over matrices emphasizes that they are expanded by including additional zero terms for size consistency purposes. Additionally, the following definition for $\bar{\mathbf{P}}$ vector is utilized:

$$\bar{\mathbf{P}}=\begin{pmatrix}\mathbf{P}^T & \boldsymbol{\Phi}_1^T & \dots & \boldsymbol{\Phi}_N^T & \boldsymbol{\Phi}_{N+1}^T \\ \dots & \boldsymbol{\Phi}_{N+M-1}^T & \mathbf{P}^{iT}\end{pmatrix}^T. \tag{51}$$

It should be mentioned that the difference between $\bar{\mathbf{P}}$ and $\mathbf{P}_I$ vectors is merely the additional pressure degree of freedom in $\mathbf{P}^T$ part of the former vector (i.e., it includes all nodes in the reservoir domain except the ones on the impounding water surface). Moreover, it is now apparent based on Eq. (50) that the proposed

$$\begin{pmatrix} -\omega^2\mathbf{M}+(1+2\beta i)\,\mathbf{K} & -\bar{\mathbf{B}}^T \\ -\omega^2\bar{\mathbf{B}} & -\omega^2\left(\bar{\mathbf{G}}+\bar{\mathbf{M}}_I\right)+i\omega\left(q\bar{\mathbf{L}}_{II}+\bar{\mathbf{C}}_I\right)+\left(\bar{\mathbf{H}}+\bar{\mathbf{K}}_I\right) \end{pmatrix} \begin{pmatrix} \mathbf{r} \\ \bar{\mathbf{P}} \end{pmatrix} = \begin{pmatrix} -\tilde{\mathbf{M}}\mathbf{J}\mathbf{a}_g \\ -\bar{\tilde{\mathbf{B}}}\mathbf{J}\mathbf{a}_g+\bar{\mathbf{F}}_I \end{pmatrix}. \quad (52)$$

Box I

approach is suitable for transient analysis. However, we should simplify this relation for time harmonic analysis, which is the main scope of present study. Under these circumstances, one may write Eq. (50) in Eq. (52) as shown in Box I. In this relation, it is assumed that the damping matrix of the dam is of hysteretic type. This means:

$$\mathbf{C}=(2\beta/\omega)\,\mathbf{K}. \quad (53)$$

5. Modeling and basic parameters

The introduced methodology is employed to analyze an idealized dam-reservoir system. The details of modeling aspects such as discretization, basic parameters, and the assumptions adopted are summarized in this section.

5.1. Models

An idealized symmetric model of Morrow Point arch dam on the rigid foundation is considered. The geometry of the dam may be found in [2]. The dam is discretized by 40 20-node isoparametric solid finite elements (Figure 2(a)).

In the case of the water domain, two strategies are adopted (Figure 2(b) and (c)). For the FE-(FE-TE) method of analysis which is our main procedure, the reservoir near-field region is discretized by fluid finite elements and the high-order boundary condition is employed on the upstream truncation boundary. This latter task is actually carried out by utilizing a truncation-element at that boundary. The length of this near-field region is denoted by L and water depth is referred to as H. A relatively low normalized reservoir length is considered herein ($L/H=1$, Figure 2(b)). This region is discretized by 200 20-node isoparametric fluid finite elements.

For the FE-(FE-HE) method of analysis, the reservoir domain is divided into two regions. The near-field region ($L/H=1$) is discretized by fluid finite elements, and the far-field region is treated by a fluid hyper-element (Figure 2(c)). Of course, it should be emphasized that this option is merely utilized to obtain the exact solution [5]. Moreover, it is well known that the results are not sensitive in this case to the normalized length of the reservoir near-field region or L/H value.

5.2. Basic parameters

The dam body is assumed to be homogeneous and isotropic with linearly viscoelastic properties for mass concrete:

- Elastic modulus (E_d) = 27.5 GPa
- Poison's ratio = 0.2
- Unit weight = 24.8 kN/m^3
- Hysteretic damping factor (β_d) = 0.05

The impounded water is taken as inviscid and compressible fluid with unit weight equal to 9.81 kN/m^3 and pressure wave velocity $c=1440$ m/sec.

6. Results

All results presented herein are obtained by the FE-(FE-TE) method discussed under GN-type high-order absorbing condition applied to the truncation boundary. The only exception is for what is referred to as the exact response. That particular case is handled by the FE-(FE-HE) analysis technique [5].

The initial part of the study is focused on the fully reflective reservoir base condition (i.e., $\alpha=1$). In this part, four different cases are considered with different orders of GN high-order truncation condition. In particular, O1-0, O1-1, O2-1, and O3-1 are utilized. Subsequently, two other cases are evaluated in which the reservoir bottom/sidewalls condition is absorptive for these models (i.e., $\alpha=0.75$). The orders O1-0 and O3-1 are employed for these cases. It is also worthwhile to mention that all traveling-type parameters of GN are taken equal ($a_j=1$). Similarly, all evanescent-type parameters of GN are also taken equal ($b_j=7.4$). This latter value is selected by a calibration strategy mentioned elsewhere for the analysis of gravity dams [22].

Figures 3 to 5 present the transfer function for radial acceleration at dam crest, i.e., corresponding to $\theta=0$ and $\theta=13.25$ (Figure 2(a)). The former is utilized for stream and vertical ground acceleration (i.e., y and z directions in Figure 2(b), symmetric excitations), and the latter for cross-stream ground motion (i.e., x direction in Figure 2(b), anti-symmetric excitation). It is noted that the response in each case is plotted versus the dimensionless frequency. The normalization of excitation frequency is carried out with respect to ω_1^s and ω_1^a for symmetric and anti-symmetric excitations, respectively. These are defined as the fundamental frequency of the dam on rigid

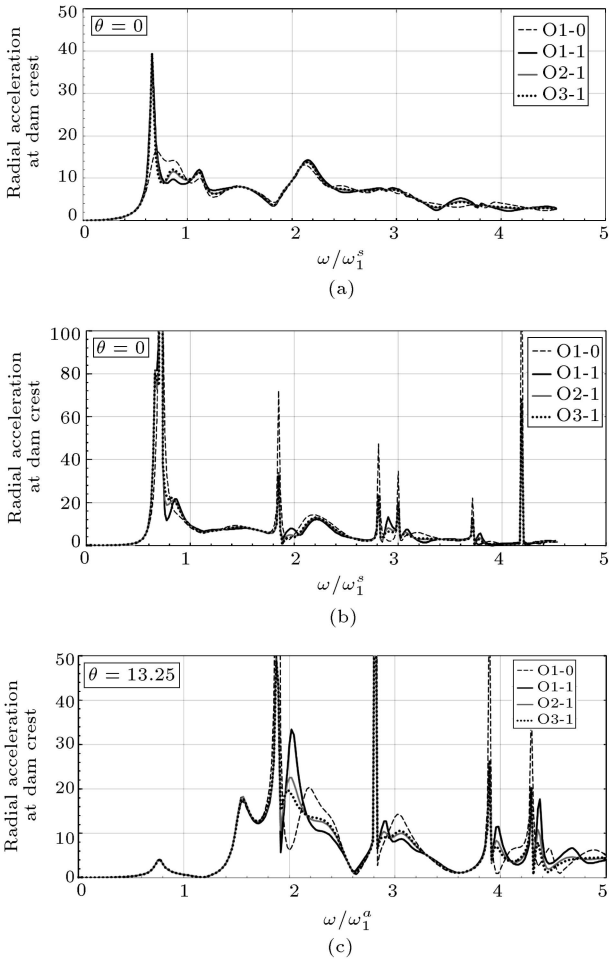

Figure 3. Radial acceleration at dam crest for different orders of GN condition due to (a) stream, (b) vertical, and (c) cross-stream excitations for the fully reflective reservoir bottom/sidewalls condition ($L/H = 1$ and $\alpha = 1$).

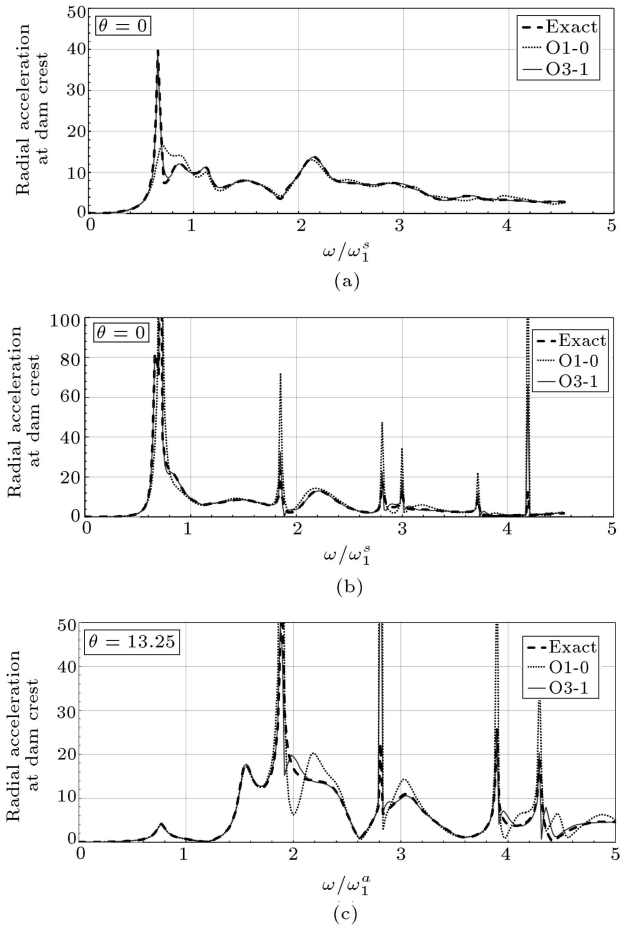

Figure 4. Radial acceleration at dam crest due to (a) stream, (b) vertical, and (c) cross-stream excitations for the fully reflective reservoir bottom/sidewalls condition ($L/H = 1$ and $\alpha = 1$); comparison between GN condition and exact results.

foundation with an empty reservoir for symmetric and anti-symmetric modes, respectively.

In this part, we considered the initial four models that relate to the fully reflective reservoir bottom/sidewalls condition (i.e., $\alpha = 1$). The responses are plotted in Figure 3. This figure shows the convergence process as order increases for all three types of excitation (i.e., stream, vertical, and cross-stream). It is noted that there is a lot of difference in responses among the first case (O1−0) and the last three cases (O*−1). This is mainly because no evanescent-type of parameter is utilized for the former case. Thus, as is included, the response at the first peak changes significantly. This is clearly observed for the latter three cases (O*−1) in comparison to the first case. Moreover, it is noticed that the overall response is very close between the last two cases (i.e., O2-1 and O3-1). This indicates that the solution has reached convergence. For a better evaluation of this claim, the response for the first and fourth cases is compared against the exact solution in Figure 4. It is to be noted that the exact solution (in numerical sense) is obtained by employing hyper-element in the model. Moreover, there are minor differences between O3-1 and exact results. Therefore, O3-1 results may actually be considered as a converged solution. There are significant errors in the O1-0 case in comparison to the exact responses, especially near the fundamental frequency of the system for symmetric excitations (stream and vertical) and after the sharp peaks (corresponding to cut-off frequencies) in the response for the anti-symmetric ground motion (cross-stream excitation).

In the second part of this study, two cases of O1-0 and O3-1 are merely considered under absorptive reservoir bottom/sidewalls condition (i.e., $\alpha = 0.75$). Similarly, these results are also compared against the exact responses for all three types of excitations in Figure 5. It is noted again that there are minor differences between O3-1 responses and exact solutions for all three types of excitations. Therefore, O3-1 results may actually be considered as the converged solution again and there is no need to consider higher

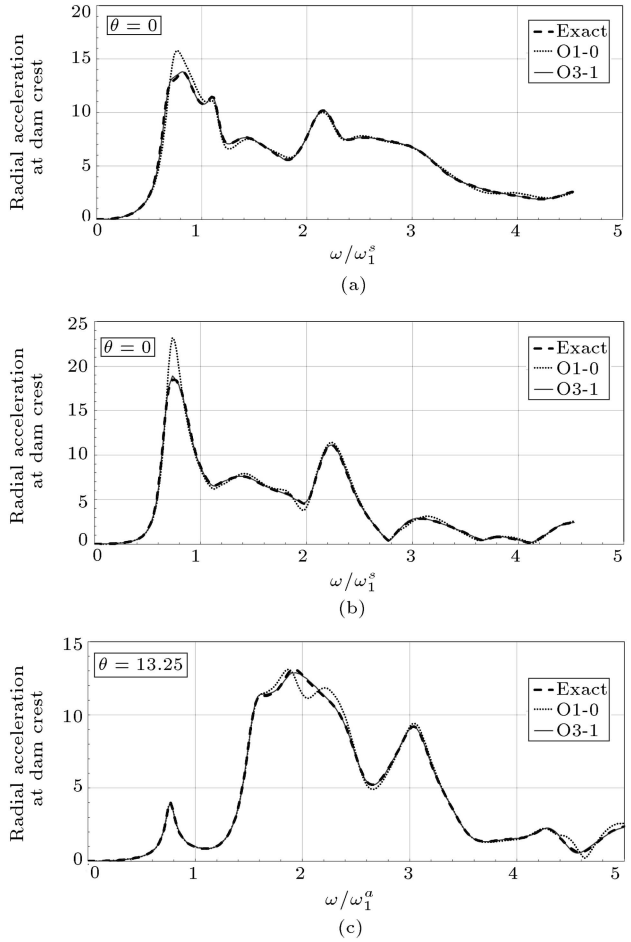

Figure 5. Radial acceleration at dam crest due to (a) stream, (b) vertical, and (c) cross-stream excitations for the absorptive reservoir bottom/sidewalls condition ($L/H = 1$ and $\alpha = 0.75$); comparison between GN condition and exact results.

orders. Moreover, it is observed that there are still errors in the O1-0 case in comparison to the exact responses, especially near the fundamental frequency of the system for symmetric excitations (stream and vertical) and after the cut-off frequencies (notice that sharp peaks diminish in the absorptive case) in the response for the anti-symmetric ground motion (cross-stream excitation). GN high-order boundary condition creates instability problems as the order gets larger. This problem occurs in this study for orders O5-1 and O4-1 under symmetric and anti-symmetric excitations, respectively. However, fortunately, O3-1 results reached convergence prior to the beginning of instability problems.

7. Conclusions

The proposed formulation based on FE-(FE-TE) procedure for dynamic analysis of concrete arch dam-reservoir system, was described in great detail. The core of the method is based on utilizing a truncation element at the U/S truncation boundary of the reservoir near-field domain while excluding the far-field region of the reservoir. This truncation element was formulated based on the GN-type high-order condition applied at that boundary. A special-purpose finite element program was enhanced for this investigation. Thereafter, the response of idealized Morrow Point arch dam was studied due to stream, vertical, and cross-stream ground motions.

Several cases were defined by changing the GN condition order. Moreover, two conditions of fully reflective (i.e., $\alpha = 1$) and absorptive (i.e., $\alpha = 0.75$) reservoir bottom/sidewalls are considered. For the fully reflective condition, four GN-condition orders of O1-0, O1-1, O2-1, and O3-1 are selected. For the absorptive reservoir study, two GN-condition orders of O1-0 and O3-1 are merely chosen. The exact results were also obtained for both reservoir bottom/sidewalls conditions and all the three types of excitations by the FE-(FE-HE) method of analysis.

Overall, the main conclusions obtained by the present study can be listed as follows:

- For the fully reflective reservoir bottom/sidewalls condition (i.e., $\alpha = 1$), minor differences were found between O3-1 and exact results. Therefore, O3-1 results might actually be considered as the converged solution. Moreover, there were significant errors in the O1-0 case in comparison to the exact responses, especially near the fundamental frequency of the system for symmetric excitations (stream and vertical) and after the sharp peaks (corresponding to cut-off frequencies) in the response for the anti-symmetric ground motion (cross-stream excitation);
- For absorptive reservoir bottom/sidewalls conditions (i.e., $\alpha = 0.75$), there were minor differences between O3-1 responses and the exact solutions for all three types of excitations. Therefore, O3-1 results might actually be considered as the converged solution and there was no need to consider higher orders. Moreover, it was observed that there were still errors in the O1-0 case in comparison to the exact responses, especially near the fundamental frequency of the system for symmetric excitations (stream and vertical) and after the cut-off frequencies in the response for the anti-symmetric ground motion (cross-stream excitation);
- It is well known that GN high-order boundary condition creates instability problems as the order becomes large. For the present study (analysis of concrete arch dam-reservoir systems), this occurs for orders O5-1 and O4-1 for symmetric and anti-symmetric excitation results, respectively. However, fortunately, O3-1 results reached convergence prior to the beginning of instability problems.

References

1. Waas, G. "Linear two-dimensional analysis of soil dynamics problems in semi-infinite layered media", Ph.D. Dissertation, University of California, Berkeley, California (1972).
2. Hall, J.F. and Chopra, A.K. "Dynamic analysis of arch dams including hydrodynamic effects", *J. Eng. Mech. Div.*, ASCE, **109**(1), pp. 149–163 (1983).
3. Fok, K.-L. and Chopra, A.K. "Frequency response functions for arch dams: hydrodynamic and foundation flexibility effects", *Earthquake Eng. Struct. Dyn.*, **14**, pp. 769–795 (1986).
4. Tan, H. and Chopra, A.K. "Earthquake analysis of arch dam including dam-water-foundation rock interaction", *Earthquake Eng. Struct. Dyn.*, **24**, pp. 1453–1474 (1995).
5. Lotfi, V. "Direct frequency domain analysis of concrete arch dams based on FE-(FE-HE)-BE technique", *Journal of Computers & Concrete*, **1**(3), pp. 285–302 (2004).
6. Sommerfeld, A., *Partial Differential Equations in Physics*, Academic press, NY (1949).
7. Sharan, S.K. "Time domain analysis of infinite fluid vibration", *Int. J. Numer. Meth. Eng.*, **24**(5), pp. 945–958 (1987).
8. Berenger, J.P. "A perfectly matched layer for the absorption of electromagnetic waves", *J. Comput. Phys.*, **114**(2), pp. 185–200 (1994).
9. Chew, W.C. and Weedon, W.H. "A 3D perfectly matched medium from modified Maxwell's equations with stretched coordinates", *Microw. Opt. Techn. Let.*, **7**(13), pp. 599–604 (1994).
10. Basu, U. and Chopra, A.K. "Perfectly matched layers for time-harmonic elastodynamics of unbounded domains: theory and finite-element implementation", *Comput. Meth. Appl. Mech. Eng.*, **192**(11-12), pp. 1337–1375 (2003).
11. Jiong, L., Jian-wei, M., and Hui-zhu, Y. "The study of perfectly matched layer absorbing boundaries for SH wave fields", *Appl. Geophys.*, **6**(3), pp. 267–274 (2009).
12. Zhen, Q., Minghui, L., Xiaodong, Z., et al. "The implementation of an improved NPML absorbing boundary condition in elastic wave modeling", *Appl. Geophys.*, **6**(2), pp. 113–121 (2009).
13. Kim, S. and Pasciak, J.E. "Analysis of Cartesian PML approximation to acoustic scattering problems in R2", *Wave Motion*, **49**, pp. 238–257 (2012).
14. Khazaee, A. and Lotfi, V. "Application of perfectly matched layers in the transient analysis of dam-reservoir systems", *Journal of Soil Dynamics and Earthquake Engineering*, **60**(1), pp. 51–68 (2014).
15. Khazaee, A. and Lotfi, V. "Time harmonic analysis of dam-foundation systems by perfectly matched layers", *Journal of Structural Engineering and Mechanics*, **50**(3), pp. 349–364 (2014).
16. Higdon, R.L. "Absorbing boundary conditions for difference approximations to the multi-dimensional wave equation", *Math. Comput.*, **47**(176), pp. 437–459 (1986).
17. Givoli, D. and Neta, B. "High order non-reflecting boundary scheme for time-dependent waves", *J. Comput. Phys.*, **186**(1), pp. 24–46 (2003).
18. Hagstrom, T. and Warburton, T. "A new auxiliary variable formulation of high order local radiation boundary condition: corner compatibility conditions and extensions to first-order systems", *Wave Motion*, **39**(4), pp. 327–338 (2004).
19. Givoli, D., Hagstrom, T., and Patlashenko, I. "Finite-element formulation with high-order absorbing conditions for time-dependent waves", *Comput. Meth. Appl. M.*, **195**(29–32), pp. 3666–3690 (2006).
20. Hagstrom, T., Mar-Or, A. and Givoli, D. "High-order local absorbing conditions for the wave equation: extensions and improvements", *J. Comput. Phys.*, **227**, pp. 3322–3357 (2008).
21. Rabinovich, D., Givoli, D., Bielak, J., et al. "A finite element scheme with a high order absorbing boundary condition for elastodynamics", *Comput. Meth. Appl. Mech.*, **200**, pp. 2048–2066 (2011).
22. Samii, A. and Lotfi, V. "High-order adjustable boundary condition for absorbing evanescent modes of waveguides and its application in coupled fluid-structure analysis", *Wave Motion*, **49**(2), pp. 238–257 (2012).
23. Lotfi, V. and Zenz, G. "Application of Wavenumber-TD approach for time harmonic analysis of concrete arch dam-reservoir systems", *Coupled Systems Mechanics*, **7**(3), pp. 353–371 (2018).
24. Lokke, A. and Chopra, A.K. "Direct finite element method for nonlinear earthquake analysis of 3-dimensional semi-unbounded dam-water-foundation rock systems", *Earthquake Eng. Struct. Dyn.*, **47**(5), pp. 1309–1328 (2018).
25. Lokke, A. and Chopra, A.K. "Direct finite element method for nonlinear earthquake analysis of concrete dams: Simplification, modeling, and practical application", *Earthquake Eng. Struct. Dyn.*, **48**(7), pp. 818–842 (2019).
26. Lotfi, V. and Lotfi, A. "Application of Hagstrom-Warburton high-order truncation boundary condition on time harmonic analysis of concrete arch dam-reservoir systems", *Engineering Computations*, **38**(7), pp. 2996–3020 (2021).
27. Mashayekhi, M. and Mostafaei, H. "Determining the critical intensity for crack initiation in concrete arch dams by endurance time method", *International Journal of Numerical Methods in Civil Engineering*, **5**(2), pp. 21–32 (2020).
28. Mostafaei, H., Ghamami, M., and Aghabozorgi, P. "Modal identification of concrete arch dam by fully automated operational modal identification", *Journal of Structures*, **32**, pp. 228–236 (2021).

29. Lotfi, V. and Sani, A.A. "Calculation of coupled modes of fluid-structure systems by pseudo symmetric subspace iteration method", *Scientia Iranica, Transactions A-Civil Engineering*, **26**(4), pp. 2100–2107 (2019).

30. Zienkiewicz, O.C., Taylor, R.L., and Zhu, J.Z., *The Finite Element Method*, Butterworth-Heinemann (2013).

31. Chopra, A.K. "Hydrodynamic pressure on dams during earthquake", *J. Eng. Mech.*, -ASCE, **93**, pp. 205–223 (1967).

32. Chopra, A.K., Chakrabarti, P., and Gupta, S. "Earthquake response of concrete gravity dams including hydrodynamic and foundation interaction effects", Report No. EERC-80/01, University of California, Berkeley (1980).

33. Fenves, G. and Chopra, A.K. "Effects of reservoir bottom absorption and dam-water-foundation interaction on frequency response functions for concrete gravity dams", *Earthq. Eng. Struct. D.*, **13**, pp. 13–31 (1985).

Biographies

Vahid Lotfi received his BS, MSc, and PhD in Civil Engineering from the University of Texas at Austin, USA. He joined Amirkabir University of Technology, Tehran, in 1986 and has been a Full Professor at that university since 2005. His research interests include finite element method, nonlinear analysis, material modeling, concrete dams, fluid-structure interaction, and soil-structure interaction.

Ali Lotfi received his BA from Amirkabir University of Technology, his MSc from University of Colorado, Denver, and his MA from University of Colorado, Boulder. He is currently a PhD candidate of Mathematics at University of Colorado, Boulder. His research interests include statistics, multicriteria optimization, nonlinear programming, applied graph theory, numerical linear algebra, data structures, and computability theory.